

Method for Thermo-optic Analysis in a Star Sensor

Hai-bo Liu[#], Ji-chun Tan, Jian-kun Yang^{*}, Xiu-jian Li, and Qing-chun Fan^{*}

School of National University of Defense Technology, Changsha, China-410 073

^{}Beijing Aerospace Automatic Control Institute, Beijing, China-100 190*

[#]E-mail: yuhan120483@yahoo.com.cn

ABSTRACT

An autonomous star sensor is a highly accurate attitude-measuring instrument used in spacecraft, and its performance is restricted by ambient temperature of the outer space. This paper puts forward an effective scheme to the thermo-optic analysis using finite element analysis (FEA) and ray tracing in star sensor. Specific difficulties: (a) how to evaluate thermo-optic effect in star sensor, and (b) how to make FEA results useful in optical design mode have been resolved using the scheme. Based on this scheme, the errors of star sensor, which are caused by thermo-optic effects, can be investigated in any complicated temperature condition, and the required temperature scope for the thermal design can be achieved. For example, the errors of the star sensor were 0.0863" and 2.2933", when the temperature differences of the experimental optical system were 10 °C and 5 °C in axial and lateral, respectively.

Keywords: Star sensor, optical system, thermo-optic analysis, finite element analysis, FEA, ray tracing

1. INTRODUCTION

An autonomous star sensor (or star tracker) is an opto-electronic instrument used to provide the absolute 3-axes attitude of a spacecraft utilising star observations¹, and it is expected to perform satisfactorily in a complicated thermal-vacuum circumstance in orbit space. But this complicated thermal circumstances unavoidably depress the performance of any optical system^{2,3}. The thermal experiments can test the performance of an optical system in star sensor, but the test results are only a holistic effect. It is hard to find the errors caused by thermo-optical effects of optical system in thermal experiments, due to the effects of noise and characteristic error of equipments. It is necessary to analyse the thermo-optic effects theoretically, and distinguish the errors caused by thermo-optical effects of optical system in a star sensor.

The thermo-optic properties of an optical system can be directly analysed only in some specific temperature conditions, such as in uniform temperature distribution^{4,5} using optical software. To analyse the thermo-optic effects in complicated temperature conditions of a star sensor, the integrated analysis process by finite element analysis (FEA) and ray tracing must be put forward⁶. However, this process is non-trivial, and two specific difficulties must be explored: (a) how to evaluate thermo-optic effect in a star sensor and (b) requirement of a coordinate space transformation because the optically relevant coordinate system is not the same as the Cartesian coordinate system typically used in the finite element model.

This paper resolves these two issues and describes an effective scheme for the integrated analysis of thermo-

optic effects on a star sensors in complicated temperature conditions.

2. EVALUATION OF THERMO-OPTIC EFFECT IN A STAR SENSOR

The optical system of a star sensor is not the same as in the general imaging system. The image plane is commonly defocused slightly from the focal plane, spreading the spot image over several pixels of a CCD camera⁷, and a sub-pixel interpolation technique is used to estimate the location of star centroid⁸. The modulation transfer function (MTF) and wavefront error are not considered appropriate to evaluate the performance of a star sensor, as these do not directly express the centroid of star image spot. So a special evaluating method is necessary for the thermo-optic effect analysis in a star sensor.

The measurement accuracy⁹ of a star sensor can be expressed as

$$\delta = \frac{A_{FOV}}{N} \times \frac{1}{\sqrt{N_{FOV}}} \times S \quad (1)$$

where, N is the number of pixels across the CCD chip, S is subpixel precision, A_{FOV} is the opening angle of optical system, and $\overline{N_{FOV}}$ is the average number of stars in the image.

The average number of stars in the image $\overline{N_{FOV}}$ is given by¹⁰:

$$\overline{N_{FOV}} = 6.57 e^{1.08M} \times \frac{1 - \cos\left(\frac{A_{FOV}}{2}\right)}{2} \quad (2)$$

where, M is the visual magnitude (M_v).

The sub-pixel precision S is determined by the hyperacuity technique algorithm that is used to determine the centroid of the star image spot⁸. So if the error of sub-pixel centroid caused by thermo-optic effect can be found, the performance of star sensor in different temperature conditions can be investigated.

Suppose that the displacement of sub-pixel centroid caused by thermo-optic effect is Δr , then:

$$\Delta r = \sqrt{(x'_0 - x_0)^2 + (y'_0 - y_0)^2} \quad (3)$$

where, (x'_0, y'_0) are coordinates of sub-pixel centroid after the changed temperature, (x_0, y_0) are coordinates of sub-pixel centroid in reference temperature.

Therefore, the error of star sensor caused by thermo-optic effect can be expressed approximately as:

$$\varepsilon = \frac{A_{FOV}}{N} \times \frac{1}{\sqrt{N_{FOV}}} \times \frac{\Delta r}{d} \quad (4)$$

where, d is the pixel size.

3. OPTICAL ANALYSIS USING FEA RESULTS

The thermo-optic analysis includes thermal and structural analysis using FEA method and optical simulation using ray tracing. However, displacements at arbitrarily located FEA nodes can not be input directly into optical software. It is desirable to have a method for transfer of the FEA results to an optical design code. Fortunately, several polynomial types including zernikes, aspheric, and XY polynomials, have been widely used in optical design program and optical testing¹¹. Before analysing optical performance, the output from FEA should be fitted using one of these polynomials.

3.1 Removal of Rigid Body Translations

For an optical system, thermal effects not only cause surface deformations of optical element, but also cause the surface translations, such as decentre, despace, and tilt as illustrated¹² in Fig.1. In the present method, the rigid body translations are removed from the surface representation.

The rigid body translations can be computed as the coordinate odd-order transformation including displacements e, f, g and deflexions $\theta_x, \theta_y, \theta_z$ of the x, y , and z . Because θ_x, θ_y , and θ_z are all small angles, the coordinate odd order transformation equation can be expressed approximately as¹³:

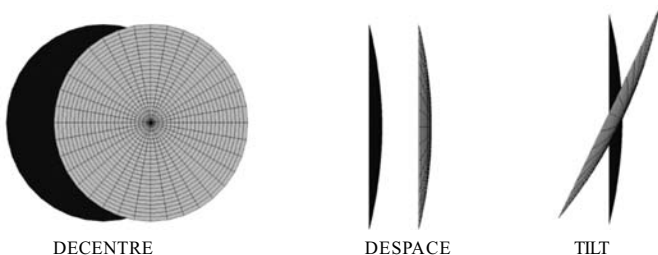


Figure 1. Decentre, despace, and tilt of optical surface.

$$\begin{bmatrix} x_i' \\ y_i' \\ z_i' \\ 1 \end{bmatrix} = T * \begin{bmatrix} x_i \\ y_i \\ z_i \\ 1 \end{bmatrix} = \begin{bmatrix} 1 & -\theta_z & \theta_y & e \\ \theta_z & 1 & -\theta_x & f \\ -\theta_y & \theta_x & 1 & g \\ 0 & 0 & 0 & 1 \end{bmatrix} * \begin{bmatrix} x_i \\ y_i \\ z_i \\ 1 \end{bmatrix} \quad (5)$$

where, T is the coordinate odd-order transformation matrix; (x_i, y_i, z_i) ($i=1,2,\dots$) are FEA nodal coordinates of original surface in reference temperature; and (x_i', y_i', z_i') are FEA nodal coordinates of deformed surface after the temperature changed. The Eqn (5) can also be written as:

$$\begin{cases} x_i' = x_i - \theta_z y_i + \theta_y z_i + e \\ y_i' = \theta_z x_i + y_i - \theta_x z_i + f \\ z_i' = -\theta_y x_i + \theta_x y_i + z_i + g \end{cases} \quad (6)$$

$$\begin{aligned} \text{Let } Q = & (x_i' - x_i + \theta_z y_i - \theta_y z_i - e)^2 + (y_i' - \theta_z x_i - y_i + \theta_x z_i - f)^2 \\ & + (z_i' + \theta_y x_i - \theta_x y_i - z_i - g)^2 \end{aligned} \quad (7)$$

The rigid body translations can be obtained by solving the extremum problem of Q .

Let $\partial Q / \partial e = 0$, $\partial Q / \partial f = 0$, $\partial Q / \partial g = 0$, $\partial Q / \partial \theta_x = 0$, $\partial Q / \partial \theta_y = 0$ and $\partial Q / \partial \theta_z = 0$. Then least square fitting approach is used to obtain the best values of rigid body translations $e, f, g, \theta_x, \theta_y, \theta_z$.

3.2 Polynomials Fitting

After the removal of the rigid body translations, the remnant FEA nodal deformations must be transferred into surface deformations acceptable by optical software. The optical surface deformations can be described in two different topological contexts: Sag-based and surface-normal (wavefront) based¹⁴. In this paper, an improved sag-based deformation is put forward to describe the surface deformations¹⁵, as shown in Fig. 2.

Assume that the function of original surface after removal of the rigid body translations is $Z_o = f(X, Y)$, one can deduce the sag-based deformation Δ_{si} in the following form:

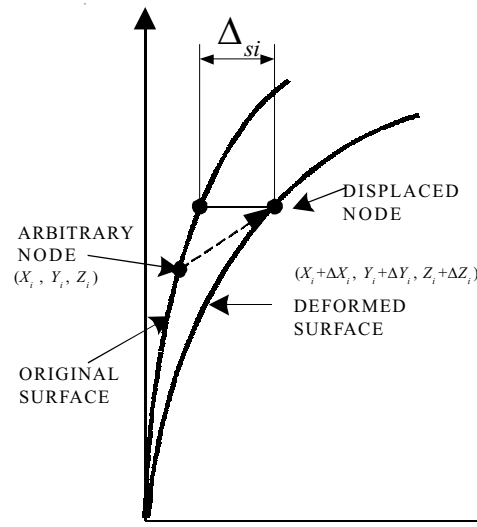


Figure 2. Schematic of surface deformation approximations.

$$\Delta_{si} = f(X_i, Y_i) + \Delta Z_i - f(X_i + \Delta X_i, Y_i + \Delta Y_i) \quad (8)$$

where,
$$\begin{bmatrix} X_i \\ Y_i \\ Z_i \\ 1 \end{bmatrix} = T * \begin{bmatrix} x_i \\ y_i \\ z_i \\ 1 \end{bmatrix} \quad (9)$$

$$\begin{bmatrix} \Delta X_i \\ \Delta Y_i \\ \Delta Z_i \\ 0 \end{bmatrix} = \begin{bmatrix} x_i \\ y_i \\ z_i \\ 1 \end{bmatrix} - T * \begin{bmatrix} x_i \\ y_i \\ z_i \\ 1 \end{bmatrix} \quad (10)$$

The XY polynomials have been widely used in optical software such as ZEMAX and CODE V. The XY polynomials are used to fit the surface deformations. So the function of deformed surface can be expressed as:

$$Z_d = f(X_i, Y_i) + \sum_{j=1}^N A_j E_j(X_i, Y_i) \quad (11)$$

where, A_j is the coefficient of polynomials, $E_j(X_i, Y_i) = (X_i/R)^m \times (Y_i/R)^n$, $j = m + n$, and R is the unitary radius. Then

$$\Delta_{si} = \sum_{j=1}^N A_j E_j(X_i, Y_i) \quad (12)$$

Substituting Eqn (12) into Eqn (8), the following result is obtained:

$$\sum_{j=1}^N A_j E_j(X_i, Y_i) = f(X_i, Y_i) + \Delta Z_i - f(X_i + \Delta X_i, Y_i + \Delta Y_i) \quad (13)$$

The values of A_j can be obtained by least square fitting approach.

4. SIMULATION OF STAR IMAGES

To evaluate the optical performance of a star sensor in different temperature conditions, the optical simulations are needed to take further analysis. Optical system such as ZEMAX can be used to simulate the detector energy on CCD by ray tracing. The star image can be simulated by ray tracing, for the starlight can be approximate to parallel lights in different field angles of view.

In the ZEMAX, the displacements e, f, g can be expressed by the surface position changes in x, y , and z . The deflexions $\theta_x, \theta_y, \theta_z$ can be expressed by the surface tilts about x, y , and z . For the surface deformations, due to the surface position can be defined⁵ by Eqn (14), it is easy to transform the A_j into ZEMAX.

$$Z = \frac{cr^2}{1 + \sqrt{1 - (1 + \kappa)c^2 r^2}} + \sum_{j=1}^N A_j E_j(X, Y) \quad (14)$$

where, c is the curvature (the reciprocal of the radius), r is the radial coordinate in lens units and κ is the conic constant.

The simulated star image spots on CCD are obtained by tracing the parallel rays using ZEMAX. When the optical system is in reference temperature, then the rigid body translations and surface deformations are transformed into ZEMAX, and the star image spots after temperature changed by tracing the same parallel rays are obtained.

After obtaining the star image spots in different

temperature conditions, one can get the sub-pixel centroids of star image spots (x'_0, y'_0) and (x_0, y_0) , respectively according to Eqn (15). The star position errors can be explored by Eqns (3) and (4).

$$x_c = \frac{\sum \sum x' I'(x', y')}{\sum \sum I'(x', y')} \quad y_c = \frac{\sum \sum y' I'(x', y')}{\sum \sum I'(x', y')} \quad (15)$$

where, (x', y') is the position of pixel (i, j) , and $I'(x', y')$ is the detected signal at pixel (i, j) .

5. THERMO-OPTIC INTEGRATED ANALYSIS

5.1 Process of Thermo-optic Analysis

The process of thermo-optic analysis for star sensor is as following:

- (a) Establish the FEA model according to structure of optical system in ANSYS; then obtain the temperature distribution by steady-state thermal analysis; calculate the deformation undergoing the temperature distribution.
- (b) Remove the rigid body translations of surface such as decentre, despace and tilt from FEA results by coordinate odd order transformation; then transfer the remnants FEA nodal deformations into XY polynomials.
- (c) Transform the surface rigid body translations and deformations into software ZEMAX; and then simulate star images on CCD by ray tracing using the non-sequential components of ZEMAX.
- (d) Calculate the centroid position based on sub-pixel interpolation algorithm; and explore star position errors and analyse the error characteristics of star sensor in different temperature distributions.

5.2 Example

An optical system used in star sensor has been analysed using the thermo-optic integrated analysis. The lens system is a 56 mm effective focal length (EFL), 11.3° field, complicated Petzval configuration, as shown in Fig. 3, and the more detailed structure parameters can be consulted in work by Xinping¹⁶. The material of barrel is TC4. The materials of lens 1, lens 3 and lens 4 in Fig. 3 are BAK6, and the materials of other lenses are all ZF2. The material parameters are shown in Table 1. The CCD is a frame-transfer device with a resolution of

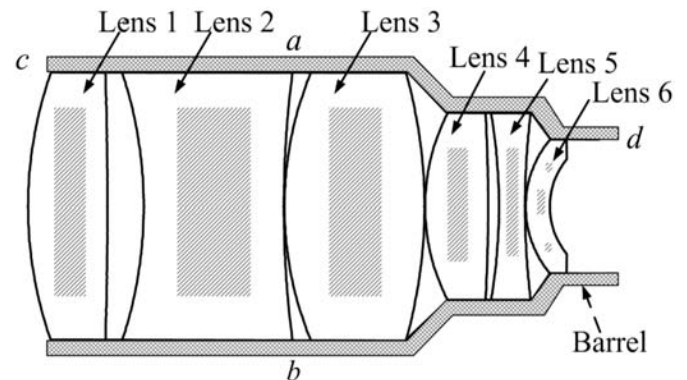


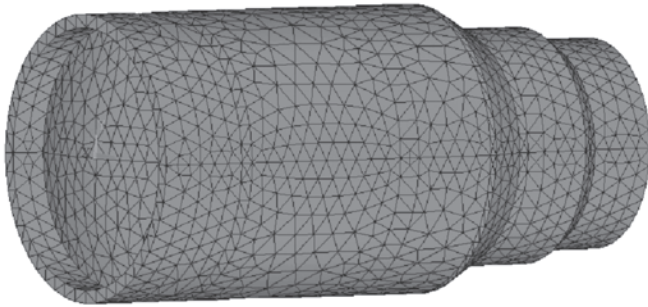
Figure 3. Structure of optical system used in a star sensor.

Table 1. Material parameters of optical system

Material	Coefficient of thermal conductivity (w/mk)	Thermal coefficient of expansion ($^{\circ}\text{C}^{-1}$)	Elastic modulus (kPa)	Poisson's ratio
TC4	6.8	9.1×10^{-6}	1.12×10^8	0.34
BAK6	1.029	6.9×10^{-6}	7.88×10^7	≈ 0.24
ZF2	0.815	8.1×10^{-6}	5.55×10^7	≈ 0.24

1024 \times 1024 pixels, each pixel being 13 $\mu\text{m} \times$ 13 μm .

With the static module of ANSYS, the structure is meshed by high precise element solid90 (20 nodes) in first step. There are 23547 elements and 37829 nodes in the model of the structure, as shown in Fig 4. In the analysis, it is presumed that the reference temperature is 20 $^{\circ}\text{C}$.


Figure 4. FEA model of optical system.

The second step of the thermo-optic analysis was steady-state thermal analysis combined with the boundary conditions. The effect of thermal contact resistance and coupled radiation are considered in this analysis. Figures 5 and 6 show two temperature distributions as an example. In the right part of the Figs 5 and 6, the temperatures of lens 1 (in Fig. 3) have been shown respectively.

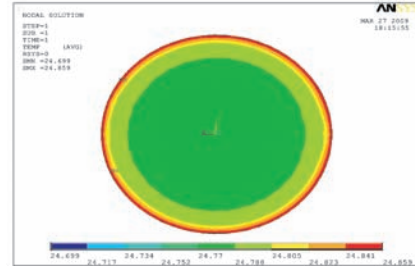
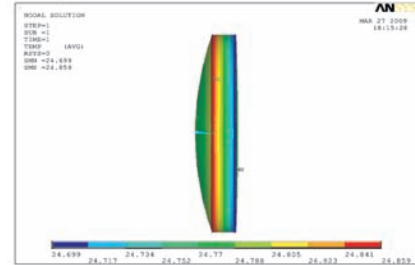
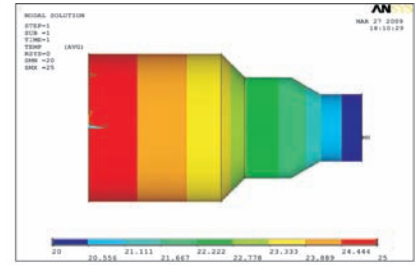
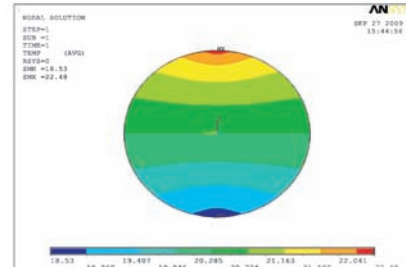
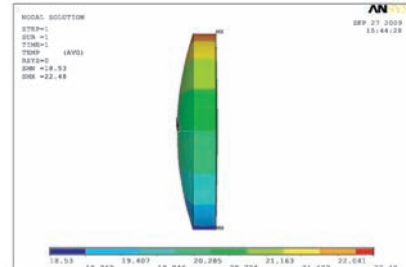
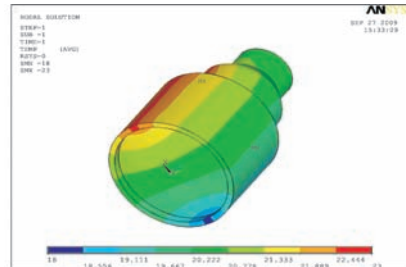
In Fig. 5, $T_{cd} = T_c - T_d$, where T_c and T_d are the temperatures of barrel's surfaces at the end c and d , respectively, as shown in Fig. 3, $T_c = 25^{\circ}\text{C}$, $T_d = 20^{\circ}\text{C}$.

In Fig. 6, $T_{ab} = T_a - T_b$, where T_a and T_b are the temperatures of barrel's outboard generatrix in side a and b , respectively, as shown in Fig. 3, $T_a = 23^{\circ}\text{C}$, $T_b = 18^{\circ}\text{C}$.

The third step was thermo-elastic analysis. The deformations were calculated undergoing the temperature field obtained in the second step, and the displacements of FEA nodes were obtained.

Figure 7 shows the deformed shape of the lens 1. The shades represent the deformed shape, and the grids represent original shape. In Fig. 7(a), the lens has despace. In Fig 7(b), the lens has not only despace but also tilt. This phenomenon is mainly caused by the elastic deformations of the barrel¹⁷.

The fourth step was calculating the rigid body translations ($e, f, g, \theta_x, \theta_y, \theta_z$) and coefficients A_j represented the surface deformations using the FEA data obtained in the third step. In this example, a third-order law XY polynomials were used to fit the surface deformations. The detailed


Figure 5. Axial temperature difference T_{cd} is 5 $^{\circ}\text{C}$.

Figure 6. Lateral temperature difference T_{ab} is 5 $^{\circ}\text{C}$.

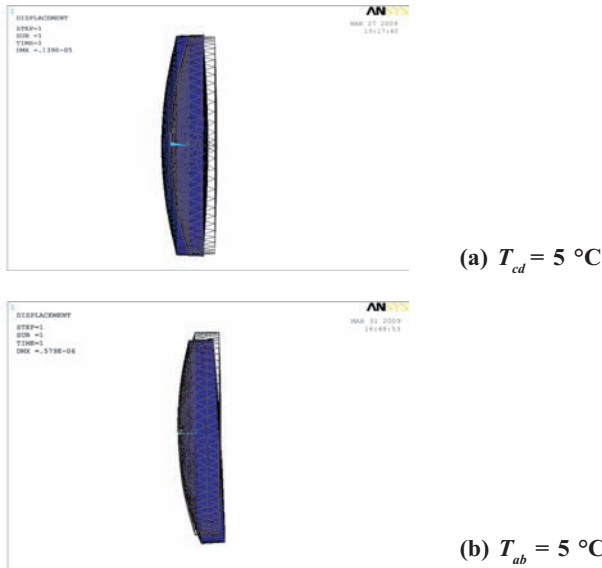


Figure 7. Deformed shapes of the lens 1.

data of the 12 surface (belonged to 6 lenses) have not been described in this paper as these are too many.

The fifth step is simulating the star image and to obtain the star spots. In this step, transform the $e, f, g, \theta_x, \theta_y, \theta_z$ and coefficients A_j of each surface into ZEMAX. Twenty star image spots in different field angles of view were obtained by ray tracing using the non-sequential components. The number of analysis parallel rays is 10^6 . It has been shown that the power of a 0 visual magnitude star is $2.94 \times 10^{-14} \text{ W/mm}^2$. Hence, the energy of parallel rays is $3.7 \times 10^{-12} \text{ W}$.

The sixth step is calculation of centroid positions of the star image spots as mentioned before and exploration of the error characteristics of star sensor in different temperature conditions. The temperature conditions and RMS errors are shown in Table 2. As shown in Table 2, the temperature distribution difference in lateral has serious effects on accuracy of the star sensor.

In this example, the thermal-optical effects have been analysed only in two types of temperature conditions, but these can be analysed in any complicated temperature condition by this method. Liu⁴, *et al.* analysed the performance of a star sensor in uniform temperatures, and Yang⁶, *et al.* analysed the image quality of optical system using ANSYS and ZEMAX, but did not investigate the centroid position

Table 2. RMS errors of star sensor in different temperature conditions

		RMS error of star position (μm)	RMS error of star sensor
Axial temperature different (T_{cd})	5 °C	0.037	0.045"
	10 °C	0.069	0.086"
Lateral temperature different (T_{ab})	2 °C	0.887	1.092"
	5 °C	1.862	2.293"

errors for a star sensor. Moreover, the effects of the barrel's thermal distortion or the lens surface thermal deformations could be investigated respectively, if only one could transform the $e, f, g, \theta_x, \theta_y, \theta_z$ or coefficients A_j into ZEMAX in the fifth step. It can provide references, not only in structure design and material choice of mechanical, but also in design of lens in a star sensor.

6. CONCLUSIONS

This paper puts forward an effective scheme to the thermo-optic analysis using FEA and ray tracing in a star sensor. Based on this scheme, the errors of star sensor can be investigated in any complicated temperature condition, and the required temperature scope for the thermal design can be achieved. It provides references in thermal control design of an optical system in a star sensor.

REFERENCES

- Schmidt, U. ASTRO APS–The next generation hi-rel star tracker based on active pixel sensor technology. *AIAA*, 2005, **5925**.
- Van, B.R.; Swanson, D.; Boyle, P.; *et al.* Flight performance of the spitzer space telescope AST-301 autonomous star tracker. *In 28th Annual AAS Rocky Mountain Guidance and Control Conference*, 2005.
- Batson, J. & Hashemi, A. Thermal deformation modeling of space optical systems with variable coefficient of thermal expansion. *In ASME Summer Heat Transfer Conference*, 2005, Vol. 4. pp. 141-49.
- Liu, Hai-Bo; Tan, Ji-Chun; Hao, Yun-Cai; *et al.* Ambient temperature effects on star sensor measurement accuracy. *Opto-electronic Engineering*, 2008, **35**(12), 40-4. [in Chinese]
- ZEMAX: Optical design program user's guide. ZEMAX Development Corporation, San Diego, CA USA.
- Yang, Dehua; Jiang, Zibo & Li, Xinna. Integrated thermal disturbance analysis of optical system of astronomical telescope. *In Modelling, Systems Engineering, and Project Management for Astronomy-III*. Vol. 7017, 2008, pp. U504-U515.
- Liu, Xinping; Cai, Xianyang; Chang, Shoude; *et al.* Bifocal optical system for distant object tracking. *Optics Express*, 2005, **13**(1), 136-41.
- Quine, B.M.; Tarasyuk, V.; Mebrahtu, H.; *et al.* Determining star-image location: A new sub-pixel interpolation technique to process image centroids. *Comp. Phys. Comm.*, 2007, **177**(9), 700-06.
- Liebe, C.C. Star trackers for attitude determination. *IEEE Aerospace Electr. Syst. Maga.*, 1995, **10**(6), 10-16.
- Liebe, C.C. Accuracy performance of star trackers-A tutorial. *IEEE Trans. Aerospace Electr. Syst.*, 2002, **38**(2), 587-99.
- Victor, L.G.; Gregory, J.M. & Keith, B.D. Making FEA results useful in optical analysis. *SPIE*, 2007, **4769**, 273-80.
- Keith, B. & Doyle, K.B. Optical modeling of finite

- element surface displacements using commercial software. *SPIE*, 2005, **5867**(1), 1-12.
13. Li, Huixian. Research and realisation of FEA post-processing in integrated optomechanical analysis. Chanchun Institute of Optics and Fine Mechanics, 2004. [in Chinese]
 14. Shan, Baozhong; Guo, Baoping; Wang, Shuyan. *In* Opto-mechanical integrated analysis for optical system. 2006. pp.1-6.
 15. Juergens, R.C. & Coronato, P.A. Improved method for transfer of FEA results to optical codes. *SPIE*, 2003, **5174**, 106-15
 16. Liu, Xinping. 56 mm lens system for mapping displacement of centroids of stars. *Acta Photonica Sinica*, 1997, **26**(7), 657-59. [in Chinese]
 17. Liu, Haibo; Hao, Yuncai; Tan, Jichun; *et al.* Effect

of Barrel's thermal deformation on measurement error of a star sensor. *Aerospace Contr. Appl. Papers*, 2008, **34**(5), 22-25, 64. [in Chinese].

Contributor



Mr Hai-bo Liu received his BS and MS from National University of Defense Technology in 2006 and 2008, respectively. His main research interests are optics and photoelectricity measurement.